RSC Advances

PAPER

View Article Online
View Journal | View Issue

Cite this: *RSC Adv.*, 2017, **7**, 5262

An anti-fouling poly(vinylidene fluoride) hybrid membrane blended with functionalized ZrO_2 nanoparticles for efficient oil/water separation

Xiang Shen,* Tiande Xie, Jiangang Wang, Peng Liu and Fan Wang

Recent advances in the fabrication of organic–inorganic hybrid membranes have received a lot of attention in membrane technology for oily wastewater treatment. In this work, a hydrophilic PVDF hybrid membrane based on poly(*N*-acryloylmorpholine)-grafted ZrO_2 nanoparticles (ZrO_2-*g*-PACMO), was prepared *via* a simple phase inversion method. PACMO was firstly grafted onto the ZrO_2 nanoparticles *via* radical polymerization, avoiding the aggregation of ZrO_2-*g*-PACMO nanoparticles that was characterized by a sedimentation test. Then, the effects of the ZrO_2-*g*-PACMO nanoparticles on the structures and performances of resultant hybrid membranes were systematically investigated. The cross-section and surface morphology of the hybrid membranes were observed by field emission scanning electron microscopy and atomic force microscopy. The results indicated that the higher concentration of ZrO_2-*g*-PACMO nanoparticles in the casting solution led to a thicker sponge-like sub-layer and a rougher surface of hybrid membranes. The prepared PVDF/ZrO_2-*g*-PACMO hybrid membrane exhibited a lower amount of adsorbed protein than that of the pristine PVDF membrane. This behavior was revealed by pure water contact angle measurement and force–extension curves. It was also found from the oil/water filtration that the total fouling (R_t) and irreversible fouling (R_{ir}) were remarkably reduced, because of the higher hydrophilicity of hybrid membranes. Furthermore, the as-prepared membranes possessed also improved separation efficiency against oil/water mixtures and the rejection ratio was as high as 99.9%. Generally, a PVDF/ZrO_2-*g*-PACMO membrane may provide potential application for efficient oil/water separation.

Received 11th November 2016
Accepted 9th December 2016

DOI: 10.1039/c6ra26651g

www.rsc.org/advances

1. Introduction

Since a significant amount of oily wastewater has been generated from many industrial processes, environmental pollution caused by the direct discharge of oily wastewaters is becoming more and more serious.[1,2] At present, there are several tools for the purification of oily wastewaters, such as air floatation, gravity separation combined skimming and biological treatments.[3–5] Among these methods, membrane separation technology has been generally accepted as an excellent method owing to its high oil-removal efficiency, low operational cost, compact design, and so on.[6,7] Polymeric materials, in particular, hydrophobic poly(vinylidene fluoride) (PVDF), are broadly used in fabricating filtration membranes to purify oily wastewaters due to their good mechanical properties as well as high well-controlled porosity and chemical resistance.[8–10] However, the serious membrane fouling can be generated by the attachment of oily foulant onto PVDF membrane surface, resulting in increased operational costs arising from the frequent membrane cleaning and membrane replacement.[11,12] Therefore, the great attentions have been paid to enhance the anti-fouling ability of PVDF membrane.

The hydrophilic modification of hydrophobic membranes is an effective way to improve the anti-fouling ability.[13,14] During separation processes, water molecules are preferentially adsorbed onto the hydrophilic membrane surface to form a hydration layer, which can effectively prevent deposition and/or adsorption of foulants.[15,16] Many hydrophilic materials, such as poly(ethylene glycol) (PEG), zwitterionic polymers and so on, have been reported on the modification of hydrophobic membrane *via* surface grafting and grafting copolymerization.[17,18] Poly(*N*-acryloylmorpholine) (PACMO) is a hydrophilic polymer with a low toxicity, and it shows a repellent property for protein adsorption.[19] Our previous studies have shown that PACMO modified PVDF membranes reveal an improved fouling resistance and hemocompatibility,[20–22] which provides a new candidate for the hydrophilic modification of membrane.

In order to modify the surface wettability of the hydrophobic membrane, an abundance of inorganic nanoparticles have been incorporated into the membrane bulks, such as titanium dioxide (TiO_2),[23,24] silicon dioxide (SiO_2),[25] aluminium oxide (Al_2O_3),[26] zinc oxide (ZnO),[27] graphene oxide (GO)[28,29] and

College of Chemistry and Environmental Science, Qujing Normal University, Qujing 655011, China. E-mail: sx008100@163.com; Fax: +86 874 8998658; Tel: +86 874 8998658

zirconium oxide (ZrO_2).[30–34] Different from TiO_2 or Al_2O_3 nanoparticles, ZrO_2 is of great interest for its excellent chemical stability, which is more suitable to fabricate hybrid membranes for the liquid-phase applications under harsh conditions.[30] Maximous *et al.*[32] reported the addition of ZrO_2 in polyethersulfone (PES) membrane. The results indicated that hybrid membranes exhibited a lower flux decline compared to the pristine PES membrane. Zheng *et al.*[33] reported on the fabrication of PVDF/ZrO_2 hybrid membranes and found that both the hydrophilicity and anti-fouling ability was stronger than those of pristine PVDF membrane. Pang *et al.*[34] also obtained similar experimental results in their investigation. Although some significative achievements have been gained, there is a pressing need to overcome some drawbacks. The agglomeration of the nanoparticles always makes it the heterogeneous distribution in the membrane matrix, leading to the decreased durability of anti-fouling ability of membranes.[35]

A key factor to render the organic–inorganic hybrid membrane with a stable fouling resistance is to increase the dispersion of inorganic nanoparticles, and to strengthen the interactions between nanoparticles and membrane matrix.[36] Encouraged by this characteristic, polymer chains can be covalently immobilized onto the nanoparticle surface, and then nanoparticles decorated with polymer chains have a good affinity with the membrane matrix.[37,38] For example, Zhang *et al.*[39] grafted hydrophilic polymer poly (2-hydroxyethyl methacrylate) (PHEMA) onto TiO_2 nanoparticles *via* the atom transfer radical polymerization (ATRP). The modified nanoparticles were found to provide remarkable enhancement in dispersion and anti-fouling ability in PVDF membrane matrix. To our knowledge, there are many investigations on the inorganic nanoparticles modified with organic polymer chains,[37–40] but introducing PACMO grafted ZrO_2 nanoparticles to fabricate hybrid PVDF membranes is rarely reported.

In this work, the nanoparticle (ZrO_2-*g*-PACMO) functionalized by hydrophilic polymer of PACMO was synthesized *via* radical polymerization. PVDF/ZrO_2-*g*-PACMO hybrid membranes were cast using different dosage of nanoparticles with a phase inversion method. The structure and performance of hybrid membranes, in terms of morphology, hydrophilicity, as well as anti-fouling ability and oil/water separation were investigated in detail. It is expected that a facile preparation of anti-fouling PVDF hybrid membrane is established.

2. Experimental

2.1 Materials

The PVDF powder (Solef 1010, $M_w = 352\,000$, $M_w/M_n = 2.3$) was purchased from Solvey Co., Ltd., (Brussels, Belgium). *N*-Acryloylmorpholine (ACMO), poly(ethylene glycol) (PEG, $M_n = 10\,000$), [3-(methacryloyloxy)propyl] trimethoxysilane (KH570), *N*,*N*-dimethyl formamide (DMF), 2,2′-azobisisobutyronitrile (AIBN), bovine serum albumin (BSA) and polyoxyethylenesorbitan monooleate (tween80) were provided by Xiyashiji Chemical Co., Ltd., (Shandong, China). High-speed vacuum pump oil (GS-1) was purchased from Beijing Sifang Special Oil Company (Beijing, China). ZrO_2 (average size of 50 nm) nanoparticles were supplied by Aladdin Reagent Co., Ltd. (Shanghai, China). The pure water (18 MΩ) used for all experiments was purified with a Milli-Q system (Millipore, America). All other chemicals, unless otherwise stated, were obtained from commercial sources and used as received.

2.2 Synthesis of ZrO_2-*g*-PACMO nanoparticles

The modification routes of nanoparticles are shown in Fig. 1. 5 g of dried ZrO_2 nanoparticles was immersed in a mixture containing 100 mL of ethanol and 100 mL of pure water, and sonicated for 30 min to produce a homogeneous suspension. 5 mL of KH570 was then added into the suspension and the reaction was conducted under nitrogen atmosphere at 40 °C for 5 h. After cooled to room temperature, the nanoparticles were collected by centrifugation and washed with ethanol to remove excess KH570. Finally, nanoparticles were dried under vacuum at 60 °C for 24 h. The obtained nanoparticles were labeled as ZrO_2–KH570.

3 g of ZrO_2–KH570 nanoparticles was dispersed in 100 mL of ethanol and sonicated for 30 min to produce a homogeneous mixture. The resultant suspension was bubbled with nitrogen for 20 min, and then 7.06 g of ACMO and 0.082 g of AIBN were introduced into the mixture. The reaction was carried out at 60 °C for 6 h. At last, the reaction mixture was washed with ethanol, centrifuged (4000 rpm, 15 min), and dried under vacuum at 60 °C for 24 h so that ZrO_2-*g*-PACMO nanoparticles were obtained.

2.3 Characterization of nanoparticles

The chemical structure of the nanoparticles was investigated by fourier transform infrared spectroscopy (FT-IR, Tensor37, Bruker, Germany). Each spectrum was captured by averaged 32 scans at a resolution of 4 cm^{-1}.

Thermogravimetric analysis was conducted on an instrument (TGA, PerkinElmer, USA) from room temperature to 1000 °C with a heating rate of 10 °C min^{-1} under nitrogen atmosphere.

The sedimentation test was used for a visual comparison between the ZrO_2 nanoparticles before and after modification. 0.1 g of ZrO_2 and/or ZrO_2-*g*-PACMO nanoparticles was placed

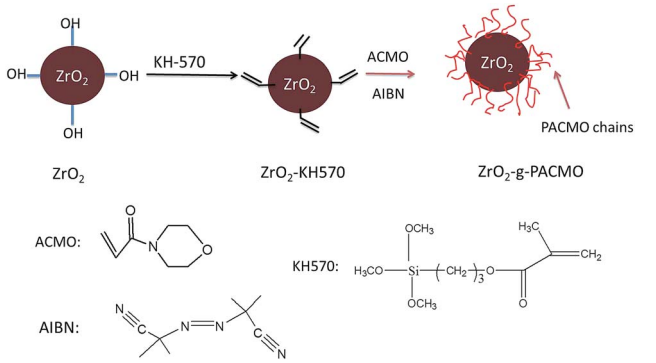

Fig. 1 Schematic illustration for synthesis of ZrO_2-*g*-PACMO nanoparticles.

into 5 mL of DMF, and ultrasonically dispersed for 30 min. After standing for 24 h, the sedimentation was recorded by digital camera (Nikon, 7200, Japan).

2.4 Preparation of PVDF/ZrO_2-*g*-PACMO hybrid membrane

PVDF/ZrO_2-*g*-PACMO hybrid membranes were fabricated *via* the phase inversion method, and the compositions of the casting solution were shown in Table 1. Measured amount of ZrO_2-*g*-PACMO nanoparticles was firstly mixed with DMF, followed by ultra-sonication for 30 min to achieve homogenous solution. The dried PVDF and PEG powder were then dissolved into the suspension and mechanically stirred at 60 °C for 6 h to produce the casting solution. After the release of any air bubbles, the solution was cast on a glass slide using a knife with a thickness of 300 μm. The liquid film was instantly immersed into 25 °C of pure water bath for the phase inversion to take place. The solid membrane was detached from the glass slide. Subsequently, the formed membrane was thoroughly rinsed with pure water to remove residual agents, and kept in pure water bath before use.

2.5 Characterization of PVDF/ZrO_2-*g*-PACMO hybrid membrane

The surface chemical compositions of membranes were determined by X-ray photoelectron spectroscopy (XPS, PHI5000C ESCA system, PHI Co., USA). The data were obtained with electron spectrometer using 300 W AlKα radiation. The core-level spectrum was calibrated by referencing to the C 1s hydrocarbon peak at 284.6 eV.

The cross-sectional structures of the membranes were probed using a field emission scanning electron microscope (FESEM, Hitachi, S-4800, Japan). The samples were fractured in liquid nitrogen to have a clean break. To prevent charging in the course of FESEM analysis, the samples was sputtered with a thin golden film before observation.

The surface morphology of membranes was observed by an atom force microscopy (AFM, CSPM5500, Benyuan-nano, China). Membrane sample was cut into a small square and attached on a glass substrate before being scanned. The surface image was then obtained with AFM analysis software in the scanning range of 5 μm × 5 μm. The surface roughness, in terms of the mean roughness (R_a), root mean square (R_q) and mean difference in the height between the highest peaks and the lowest valleys (R_z), was also studied by AFM at a scan size of 5 μm × 5 μm. The reported value for each sample was the average of at least five scans.

Table 1 The feed mass ratios of casting solutions

Membranes	PVDF (wt%)	ZrO_2-*g*-PACMO (wt%)	PEG (wt%)	DMF (wt%)
M0	15	0	5	80
M1	14	1	5	80
M2	13	2	5	80
M3	12	3	5	80
M4	11	4	5	80

The interaction force between the membrane surface and BSA-immobilized tip was detected by AMF. The AFM tip was modified according to the procedures described in the previous work.[41] Briefly, the Si_3N_4 cantilever was activated with oxygen plasma, and then chemically treated with 3-triethoxysilylpropylamine (KH550) for 2 h at room temperature. This modified tip was reacted with BSA for 30 min, followed by the cross-linkage with glutaraldehyde solution. As a result, BSA was covalently immobilized onto the cantilever. As the BSA-immobilized AFM tip approached to the membrane surface, an interaction was generated between the tip and membrane surface, resulting in a cantilever deflection. By multiplying the spring constant of the cantilever, the interaction force could be calculated. On the other hand, when the tip was retracted from membrane surface, the force could also be detected in the same manner. In the present work, all the experiments were conducted in phosphate buffer solution (PBS, pH = 7.4) at room temperature. A force–extension curve was collected from at least five positions on a sample surface.

The mean pore size of the prepared membranes was determined by Kubo-X1000 analyzer (Beijing Builder Electronic Technology Co., Ltd), which was derived from the nitrogen adsorption–desorption isotherms using the Barrett–Joyner–Halenda (BJH) model.[20] After nitrogen was admitted into the membrane chamber in controlled increments, the volume of adsorbed nitrogen was calculated. Subsequently, the pore size was obtained by extending the process that condensed the nitrogen into the membrane pores. The reported value was the average of at least three measurements for each membrane.

The overall porosity (ε) was determined by the gravimetric method,[42] as calculated by the following equation:

$$\varepsilon = \frac{w_1 - w_2}{A \times l \times \rho} \times 100\% \quad (1)$$

where w_1 and w_2 are the weights of the wet and dry membrane, respectively. A represents the membrane effective area (m^2), ρ is the water density and l denotes the membrane thickness (m).

2.6 Protein adsorption

The static BSA adsorption was conducted to evaluate the anti-fouling property of hybrid membranes. As-prepared membranes were cut into regular shape of 2 cm × 2 cm and immersed into 10 mL of BSA (0.5 g L^{-1}) solution. After oscillating incubation for 24 h at 25 °C to reach adsorption equilibrium, concentration of BSA solution after adsorption was determined by measuring the absorbance at 280 nm. The adsorption mass was calculated on the basis of the changed concentrations of BSA solution before and after adsorption. Triplicate samples for each membrane were tested to obtain the mean values.

2.7 Water contact measurements

The surface wettability of membrane was evaluated by a contact angle instrument (DSA100, Krüss, Germany). 5 μL of pure water drop was dripped onto the membrane surface and the process was recorded by video camera. The values of contact angle were obtained using the drop shape image analysis system.

2.8 Oil/water separation experiments

1 g of vacuum pump oil (GS-1) and 0.1 g of tween80 were immersed into 1000 mL of pure water, and the resultant mixture was sonicated at a power of 2 kW for 30 min to prepare the oil/water mixture. The oil/water separation performance of membranes was evaluated *via* a filtration system described in our previous work.[20] Each membrane was initially pressurized at 0.2 MPa for 30 min, and then the pressure was lowered to 0.1 MPa. The water flux at 0.1 MPa, $J_{w,1}$ (L m^{-2} h^{-1}), was calculated by the eqn (2):

$$J = \frac{V}{A \times \Delta t} \quad (2)$$

where V (L) was the volume of permeated pure water, A (m^2) and Δt (h) represented the effective area of membrane and permeation time, respectively. In the following step, the feed solution reservoir was emptied and refilled with oil/water mixture. The flux of oil/water mixture, J_p (L m^{-2} h^{-1}), was achieved based on the water quantity permeating the membranes. The oil rejection ratio was calculated by the following eqn (3):

$$R = \frac{C_f - C_p}{C_f} \times 100\% \quad (3)$$

where C_f and C_p are the concentration of oil in the feed and permeate solution, respectively. The concentration was obtained from the absorbance determined by UV-spectrophotometer (UV-1601, Shimadzu, Japan) at 530 nm. After the filtration process of oil/water mixture, the membranes were flushed with pure water for 30 min. The pure water flux of cleaned membranes, $J_{w,2}$ (L m^{-2} h^{-1}), was measured again. The flux recovery ratio (FR) in the filtration process was calculated using the following expression (4):

$$\mathrm{FR}\ (\%) = \frac{J_{w,2}}{J_{w,1}} \times 100 \quad (4)$$

In order to further evaluate the anti-fouling ability of membranes during the filtration process, three parameters, including the reversible fouling ratio (R_r), irreversible fouling ratio (R_{ir}) and total fouling ratio (R_t), were calculated by the following expressions:

$$R_r\ (\%) = \frac{J_{w,2} - J_p}{J_{w,1}} \times 100 \quad (5)$$

$$R_{ir}\ (\%) = \frac{J_{w,1} - J_{w,2}}{J_{w,1}} \times 100 \quad (6)$$

$$R_t\ (\%) = \frac{J_{w,1} - J_p}{J_{w,1}} \times 100 \quad (7)$$

3. Results and discussions

3.1 Modification and characterization of nanoparticles

ZrO_2 nanoparticles were modified by radical grafting polymerization. The C=C double bonds were immobilized on ZrO_2 surface by coupling with KH570 to form ZrO_2–KH570 nanoparticles. Poly(*N*-acryloylmorpholine) (PACMO) chains were then grafted onto the ZrO_2–KH570 *via* radical polymerization. The resultant nanoparticles, denoted as ZrO_2-*g*-PACMO, were obtained.

3.1.1 FT-IR analysis. The chemical structures of ZrO_2, ZrO_2–KH570 and ZrO_2-*g*-PACMO nanoparticles were investigated *via* FT-IR spectra, and the result was shown in Fig. 2. A broad absorption peak at 3420 cm^{-1}, is assigned to the stretching vibration of –OH groups on the ZrO_2 nanoparticle surface.[43] The ZrO_2–KH570 spectrum shows a strong peak at 1720 cm^{-1}, which is associated with the ester carbonyl (O–C=O) of KH570. Compared with ZrO_2–KH570 particle, ZrO_2-*g*-PACMO spectrum exhibits a peak at 1446 cm^{-1} that is attributed to the stretching vibrations of C–N from the PACMO. Furthermore, the peaks at 1114 cm^{-1} and 1230 cm^{-1} are ascribed to the stretching vibrations of C–O–C within morpholine ring of PACMO.[20,21] The FT-IR results prove qualitatively the presence of PACMO chains on the nanoparticle surface.

3.1.2 TGA analysis. The PACMO content of ZrO_2-*g*-PACMO nanoparticles was investigated by TGA analysis as shown in Fig. 3. It is found that the weight loss curves are almost stable when the temperature is higher than 700 °C. According to the residue, the weight loss of ZrO_2–KH570 is about 0.78% and the decreased value of ZrO_2-*g*-PACMO nanoparticles is 1.46% as compared with ZrO_2 nanoparticles. This result indicates that the weight percentage of grafted PACMO onto the ZrO_2–KH570 nanoparticles is 0.68%.

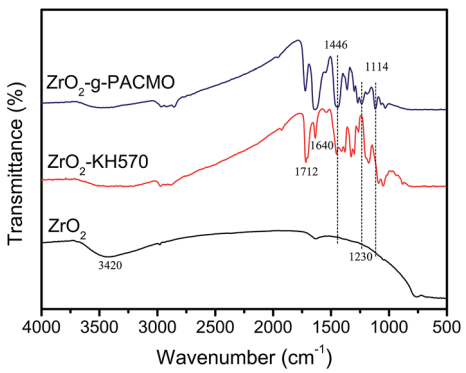

Fig. 2 FT-IR spectra of ZrO_2, ZrO_2–KH570 and ZrO_2-*g*-PACMO nanoparticles.

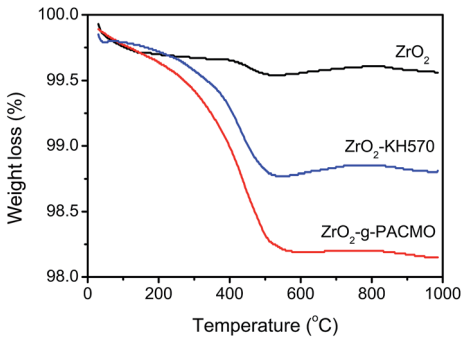

Fig. 3 TGA curves of ZrO_2, ZrO_2–KH570 and ZrO_2-*g*-PACMO nanoparticles.

3.1.3 Sedimentation test. Since DMF is one of the commonly used solvents for PVDF membrane fabrication, it is selected to evaluate the dispersion of ZrO_2 and ZrO_2-*g*-PACMO nanoparticles. As shown in Fig. 4, sedimentation tests suggest that the pristine ZrO_2 rapidly settled down, whereas the ZrO_2-*g*-PACMO nanoparticles is still suspending in DMF after 24 h. It is a remarkable behavior by contrast with sedimentation test that PACMO surface-grafting can significantly improve the dispersion status of ZrO_2 in the organic phase.

3.2 Chemical composition of hybrid membrane surfaces

The hybrid membranes were prepared using conventional immersed phase inversion. Fig. 5 shows the XPS wide-scan spectra of membrane surfaces. Only two signals at 687.3 eV and 285.7 eV, corresponding to F 1s and C 1s respectively, can be observed on the pristine PVDF membrane surface (M0). On the other hand, additional four emissions are detected at 532.3 eV, 400.6 eV, 181.1 eV and 100.1 eV, which are assigned to the O 1s, N 1s, Zr 3d and Si 2p on the hybrid membrane surface (M4), respectively. The atom percentages of membrane surface were summarized in Table 2. The percentages of N 1s, O 1s and Zr 3d increase with the increasing mass ratio of ZrO_2-*g*-PACMO, which confirms that the distribution of ZrO_2-*g*-PACMO on the membrane surface is dependent on the feed concentration of ZrO_2-*g*-PACMO in the casting solution.

3.3 Morphologies of hybrid membranes

Cross-sectional structures of membranes prepared from PVDF/ZrO_2-*g*-PACMO/PEG/DMF systems with different contents of ZrO_2-*g*-PACMO additives are shown in Fig. 6 (left column). The pristine PVDF membrane (M0) presents a typical asymmetric structure consisting of a thin skin layer and a porous finger-like sub-layer. The finger-like structure is interconnected with the membrane bulks. However, the PVDF/ZrO_2-*g*-PACMO hybrid membranes exhibit strong change in the sub-layer structure. With the increase of ZrO_2-*g*-PACMO in casting solution, the finger-like structure is suppressed and a thick sponge-like structure is observed near the bottom side. Bian and coworkers obtained similar results in the preparation of PVDF/TiO_2 membranes.[24] In comparison to unmodified nanoparticles, the PACMO grafted ZrO_2 nanoparticles is compatible with PVDF backbones in the casting solution.[39] This increase in compatibility may decrease the diffusion rate of nonsolvent. A delayed demixing process is then generated, resulting in the suppression of finger-like structure and development of sponge-like sub-layer during membrane formation.

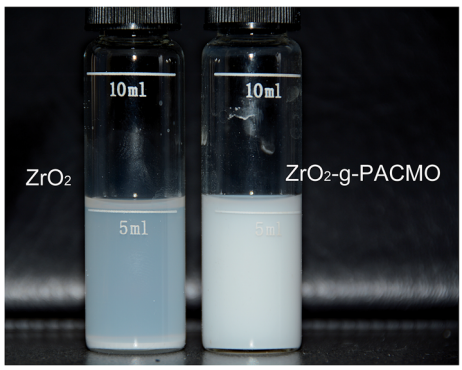

Fig. 4 Sedimentation tests of ZrO_2 and ZrO_2-*g*-PACMO nanoparticles in DMF after 24 h.

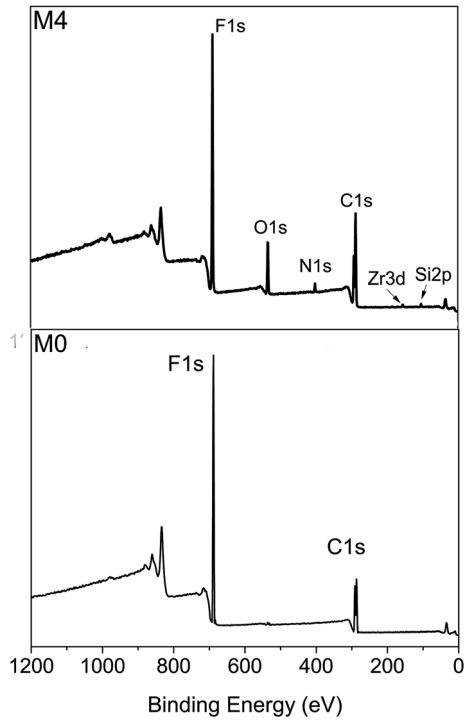

Fig. 5 XPS wide-scan spectra of pristine PVDF membrane (M0) and hybrid membrane (M4).

Table 2 Chemical elemental concentrations of membrane surfaces

Sample	C 1s (%)	F 1s (%)	O 1s (%)	N 1s (%)	Si 2p (%)	Zr 3d (%)
M0	51.49	45.63	2.88	—	—	—
M1	54.07	37.75	4.24	1.32	1.36	1.26
M2	54.70	34.10	6.09	1.55	1.73	1.83
M3	55.18	30.43	7.76	1.78	2.50	2.35
M4	57.79	25.03	9.43	2.27	2.66	2.82

The surface morphology of pristine PVDF membrane (M0) and hybrid membranes (M1, M2, M3 and M4) was evaluated by three-dimensional AFM images. As shown in Fig. 6 (right column), the bright and dark areas represent to peaks and valleys on the membrane surface, respectively. In order to further investigate the surface variations, mathematical analysis of the AFM images was conducted. The parameters, R_a, R_q and R_z, represent the mean roughness, root mean square and mean difference in the height between the highest peaks and the lowest valleys, respectively. As evident from Table 3, pristine PVDF membrane exhibits the lowest roughness, which confirms the visual observation in Fig. 6. The numerical values of R_a, R_q and R_z of hybrid membranes are much higher than that of

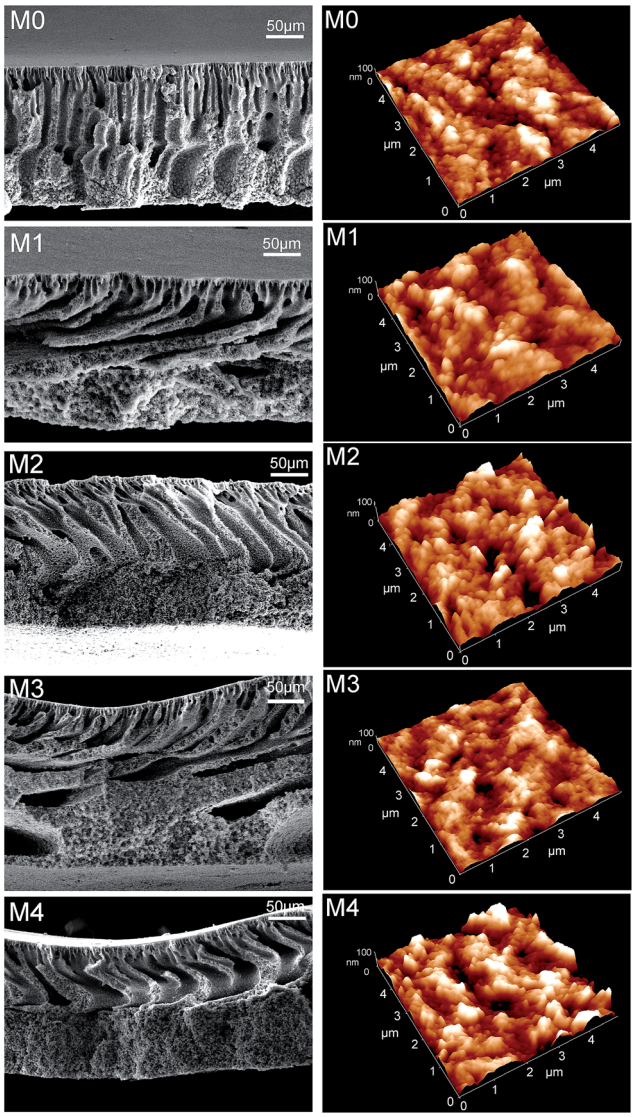

Fig. 6 Morphologies of pristine PVDF membrane (M0) and hybrid membranes (M1, M2, M3 and M4). Left column: cross-sections of membranes; right column: three-dimensional AFM images of membrane surfaces.

Table 3 Roughness parameter, mean pore size and porosity of hybrid membranes

Sample	R_a (nm)	R_q (nm)	R_z (nm)	ε (%)	r_m (nm)
M0	12	20	138	77.6	31.6
M1	16	21	139	70.4	25.8
M2	19	25	152	68.1	23.2
M3	22	29	181	62.3	20.6
M4	30	38	217	58.4	17.0

pristine PVDF membrane. These results indicate that the addition of ZrO_2-*g*-PACMO nanoparticles renders the membrane with a rough surface structure. High surface roughness can increase the effective filtration area, which leads to the enhancement of pure water flux ultimately.[45]

The mean pore size and porosity information for hybrid membranes were also listed in Table 3. With the increase of ZrO_2-*g*-PACMO in the casting solution, the mean pore size and porosity of membranes decrease from 31.6 nm and 77.6% to 17.0 nm and 58.4%, respectively. Similar experimental results were obtained previously by Zhang and coworkers for the PVDF/attapulgite hybrid membrane fabricated with phase inversion method.[44] As organic shrinkage occurs during the precipitation process of wet-casting polymeric membranes, the increase in stress between the PVDF and ZrO_2-*g*-PACMO endows the membrane with low porosity and mean pore size. Another possibility is the pore blockage due to the precipitation of ZrO_2-*g*-PACMO on the pore wall, leading to the decrease in the pore size and porosity. It is noteworthy that the mean pore size of membranes seems much smaller than that of the membrane surface observed in AFM images (Fig. 6). The distinct differences between these data may be explained that only the size in the range of 2–100 nm can be measured under the adsorption–desorption experiments.[20]

3.4 Anti-fouling ability of hybrid membranes

The fouling resistance of membrane was related with the protein adsorbed onto the membrane surface. In the present study, the BSA was selected to evaluate the anti-fouling ability of the prepared membranes. BSA adsorption amounts of membranes with different concentrations of ZrO_2-*g*-PACMO nanoparticles are indicated in Fig. 7. The adsorbed BSA amount reduces with addition of ZrO_2-*g*-PACMO, and the amount is about 43.7 μg cm^{-2} when the incorporated ZrO_2-*g*-PACMO nanoparticle is 4%. The adsorption amount is decreased by 58.7% as compared with pristine PVDF membrane. These results demonstrate that the incorporation of ZrO_2-*g*-PACMO nanoparticles can efficiently prevent protein adsorption.

The surface hydrophilicity was determined to evaluate the anti-fouling behavior of the prepared hybrid membranes. The dynamic pure contact angles of the membranes were shown in Fig. 8. The initial water contact angle of the pristine PVDF membrane (M0) is as high as 93° because of its high hydrophobicity. After the incorporation of ZrO_2-*g*-PACMO nanoparticles, the contact angle of hybrid membranes reduces gradually along with the ZrO_2-*g*-PACMO concentration increasing. The contact angles of membranes are reduced to

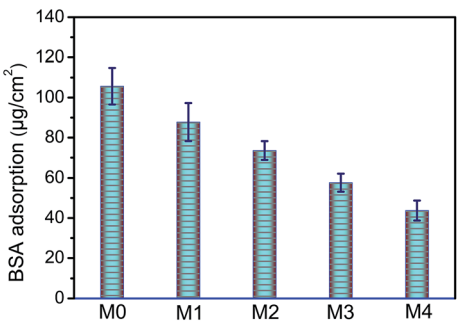

Fig. 7 The amount of BSA adhered to pristine PVDF membrane (M0) and hybrid membranes (M1, M2, M3 and M4).

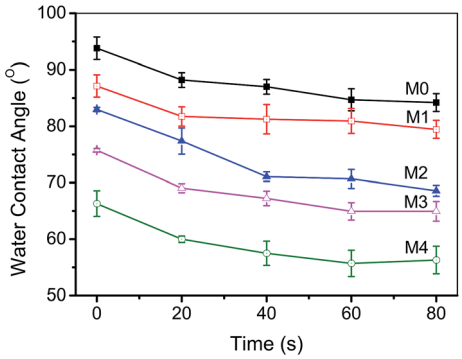

Fig. 8 Water contact angles of pristine PVDF membrane (M0) and hybrid membranes (M1, M2, M3 and M4).

89°, 86°, 78° and 66°, corresponding to M1, M2, M3 and M4, respectively. It is obvious that the hydrophilicity of membrane is enhanced as result of the addition of ZrO_2-*g*-PACMO in the casting solution. This behavior is ascribed to the fact that the PACMO grafted ZrO_2 nanoparticles are distributed on the membrane surface during the membrane formation.[46] When a water droplet is dripped onto the hybrid membrane surface, it can be spread because of hydration capability of PACMO for water molecules.

The adhesion force of foulants against the membrane surface is a critical parameter that allows direct evaluation of anti-fouling behavior at the interface.[47] Previous works also confirmed that the fouling inclination of the membrane surface is well consistent with the magnitude of adhesion force.[48] In this work, the interaction force between membrane surface and BSA macromolecules was measured *via* AFM to further investigate the anti-fouling mechanism. As shown in Fig. 9, the adhesion forces between hybrid membranes (M1, M2, M3 and M4) and BSA are 13.8 nN, 8.0 nN, 5.1 nN and 2.6 nN, which is much lower than 23.0 nN of pristine PVDF membrane (M0). Upon considering the adsorbed BSA amounts of membranes, it is obvious that, the weaker the adhesion force of the membrane-BSA, the lower amounts of protein adsorbed to membrane surface. In another word, a hydration layer is formed on the membrane surface and then prevents the protein adsorption due to the addition of ZrO_2-*g*-PACMO. This result also indicates that the membrane fouling can be inhibited *via* the elimination of foulant-membrane adhesion force.

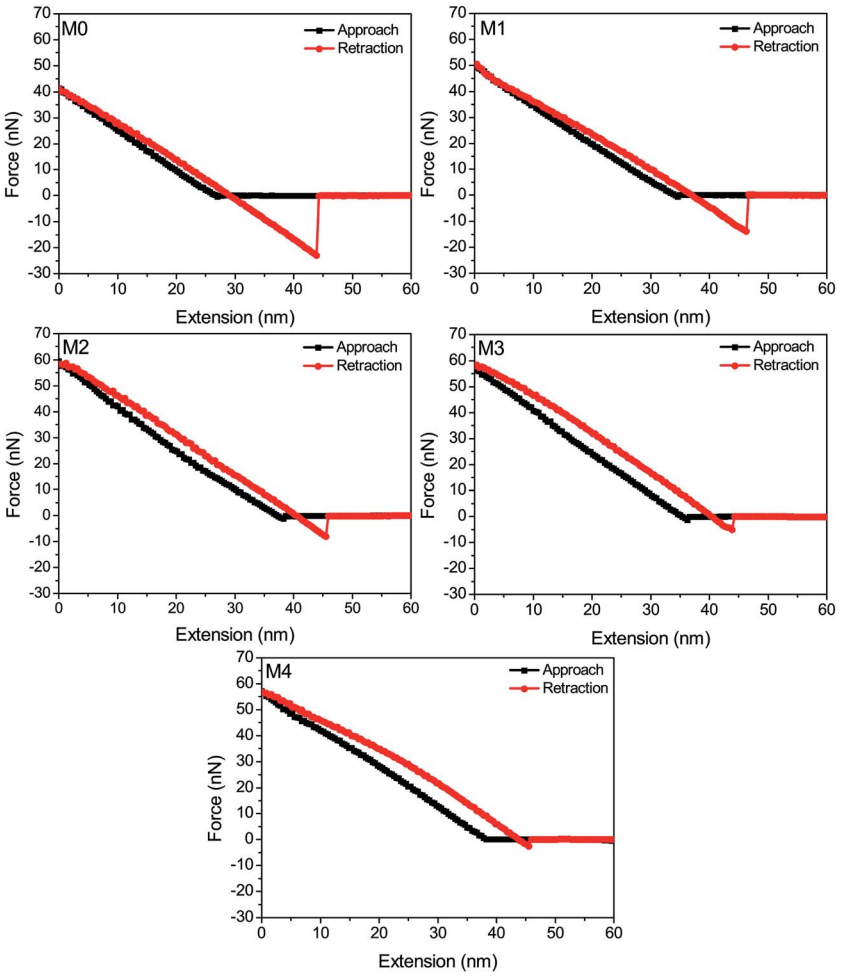

Fig. 9 Force-extension curves recorded with a BSA-immobilized tip against pristine PVDF membrane (M0) and hybrid membranes (M1, M2, M3 and M4).

3.5 Oil/water separation performance of hybrid membranes

Cycle filtration was conducted to evaluate the permeation performance of the prepared membranes. The first stage was the pure water filtration through the membranes. The second step was the filtration of oil/water mixture, and the third stage was the steady permeation of pure water after simple washing with pure water. The permeated solution in each stage was collected and the fluxes could be calculated by eqn (2). As shown in Fig. 10, the pure water flux and oil/water flux are significantly affected by the content of ZrO_2-*g*-PACMO nanoparticles in the casting solution. The pristine PVDF membrane (M0) exhibits the lowest pure water flux and oil/water flux around 36.2 L m^{-2} h^{-1} and 8.9 L m^{-2} h^{-1}. The flux values increase when the concentration of ZrO_2-*g*-PACMO nanoparticles increases from 1% to 4%. During the filtration of oil/water solution, the rejection ratio of membrane was also measured and the result was shown in Fig. 11. It is found that the rejection ratio exhibits the same propensity with the flux change. Especially for hybrid membrane M4, the value is as high as 99.9%, indicating an efficient separation of oil/water mixture. In general, the permeation performance is dependent on the porosity, mean pore size and hydrophilicity of the membrane.[35] In the present work, the decreased pore size and improved hydrophilicity of membranes are the dominated factors affecting the fluxes and rejections. Obviously, the improved surface hydrophilicity can reduce the interfacial resistance and promote water molecules to pass through the membrane pores, which would efficiently increase the fluxes of membranes.[49] The addition of ZrO_2-*g*-PACMO nanoparticles endows the prepared hybrid membranes (M1, M2, M3 and M4) with a smaller pore size than pristine PVDF membrane. Thus, the dense membrane surface makes the oil droplets difficult to permeate through membrane matrix. On the other hand, the compact hydration layer also resists oil droplets to adsorb on the membrane surface and to pass through membrane.

The anti-fouling ability of membranes during filtration process was quantitatively investigated in detail. On the basis of the fluxes data, total fouling ratio (R_t), irreversible ratio (R_{ir}) and reversible fouling ratio (R_r) were calculated. As given in Fig. 12, R_t value of the pristine PVDF membrane (M0) is highest at 75.3%, indicating serious flux decline caused by oil fouling. In comparison to pristine PVDF membrane, the R_t values for hybrid membranes (M1, M2, M3 and M4) reduce to 47.9%, 44.2%, 41.5% and 37.4%, respectively. Furthermore, the flux recovery ratio (FR) and R_r/R_{ir} value of as-prepared membranes were shown in Fig. 13. The increase of R_r/R_{ir} value confirms that the irreversible membrane fouling is converted into reversible membrane fouling in the filtration process. In another word, the irreversible oil fouling on the membrane surface is inhibited due to the incorporation of ZrO_2-*g*-PACMO nanoparticles. This result is ascribed to the fact that the formed hydration layer can reduce the interaction force between membrane surface and oil droplet, leading to the prevention of irreversible oil adhesion. The flux recovery ratio (FR) displayed in Fig. 13 can

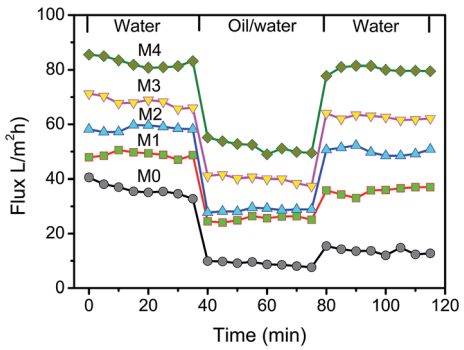

Fig. 10 Time-dependent fluxes of pristine PVDF membrane (M0) and hybrid membranes (M1, M2, M3 and M4).

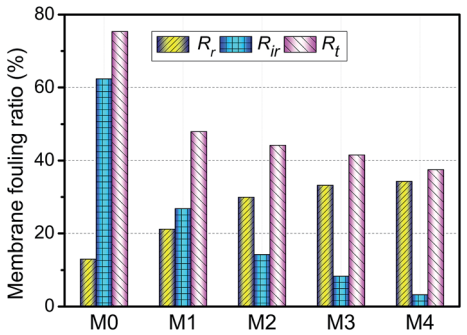

Fig. 12 Total fouling ratio (R_t), irreversible ratio (R_{ir}) and reversible fouling ratio (R_r) for pristine PVDF membrane (M0) and hybrid membranes (M1, M2, M3 and M4) during the cycle filtration.

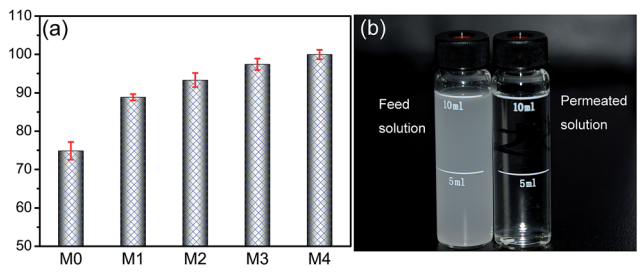

Fig. 11 (a) Rejection of the oil/water solution for pristine PVDF membrane (M0) and hybrid membranes (M1, M2, M3 and M4); (b) photograph of oil/water mixture before and after permeation through M4 hybrid membrane.

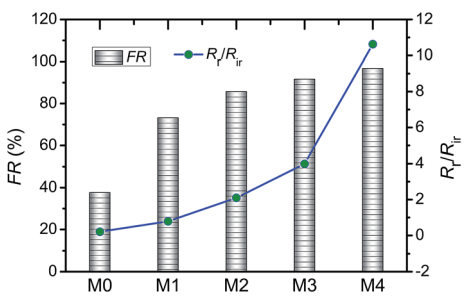

Fig. 13 Flux recovery ratio (FR) and R_r/R_{ir} value of pristine PVDF membrane (M0) and hybrid membranes (M1, M2, M3 and M4) during the cycle filtration.

obviously present the suitable recycling performance of the PVDF/ZrO_2-*g*-PACMO membranes. The hybrid membrane exhibits a higher flux recovery than pristine PVDF membrane. As for hybrid membrane M4, the flux recovery ratio reaches to 97%. This is originated from the hydrophilic effect of grafted PACMO chains. In addition, the well dispersed ZrO_2-*g*-PACMO in the membrane pore channel makes the entrapped oil droplets in the membrane pores to be removed easily by water flushing.[50] These results suggest that incorporation of ZrO_2-*g*-PACMO nanoparticles also enhances the oil fouling resistance in the filtration process.

4. Conclusions

In this work, PACMO grafted ZrO_2 nanoparticles (ZrO_2-*g*-PACMO) were successfully synthesized *via* radical polymerization. The PVDF/ZrO_2-*g*-PACMO hybrid membranes were fabricated *via* phase inversion method. The effects of ZrO_2-*g*-PACMO concentration on the morphology, anti-fouling ability and oil/water separation performance of membranes were investigated in detail. It was found from sedimentation test that the synthesized ZrO_2-*g*-PACMO nanoparticles could be uniformly dispersed in organic solvent DMF. With the increase of ZrO_2-*g*-PACMO nanoparticles in the casting solution, the finger-like structures at the cross-sections of PVDF/ZrO_2-*g*-PACMO membranes were suppressed and the sponge-like layers were gradually formed. Compared with pristine PVDF membrane, the incorporation of ZrO_2-*g*-PACMO nanoparticles led to the decrease of mean pore size and porosity, and the formation of rougher membrane surface. The adsorbed BSA protein to hybrid membranes was much lower than that of pristine PVDF membrane, which was resulted from the increase of surface hydrophilicity and the decrease of interaction force between membrane surface and foulants. The prepared PVDF/ZrO_2-*g*-PACMO exhibited an effective separation of oil/water solution and the rejection ratio was as high as 99.9%. Cycle filtration process showed that ZrO_2-*g*-PACMO nanoparticles were a good modifier for the formation of anti-fouling PVDF membrane.

Acknowledgements

This research is financially supported by Yunnan Applied Basic Research Projects of China (Grant No. 2015FD047), Yunnan Provincial Department of Education Research Foundation (Grant No. 2015Y433), and Innovation Training Program of Chinese College Students (Grant No. 201510684004 and 201610684007). The authors wish to acknowledge Prof. Li Chen and Prof. Yiping Zhao for membrane characterization at Tianjin Polytechnic University of China.

References

1 D. Sarkar, D. Datta, D. Sen and C. Bhattacharjee, *Chem. Eng. Sci.*, 2011, **66**, 2554–2567.
2 A. Asatekin and A. M. Mayes, *Environ. Sci. Technol.*, 2009, **43**, 4487–4492.
3 S. Cappello, A. Volta, S. Santisi, C. Morici, G. Mancini, P. Quatrini, M. Genovese, M. M. Yakimov and M. Torregrossa, *Int. Biodeterior. Biodegrad.*, 2016, **110**, 235–244.
4 C. Yeom and Y. Kim, *J. Ind. Eng. Chem.*, 2016, **40**, 47–53.
5 P. Painmanakul, P. Sastaravet, S. Lersjintanakarn and S. Khaodhiar, *Chem. Eng. Res. Des.*, 2010, **88**, 693–702.
6 J. P. Ju, T. M. Wang and Q. H. Wang, *Colloids Surf., A*, 2015, **481**, 151–157.
7 X. F. Gao, L. P. Xu, Z. X. Xue, L. Feng, J. T. Peng, Y. Q. Wen, S. T. Wang and X. J. Zhang, *Adv. Mater.*, 2014, **26**, 1771–1775.
8 Y. Z. Zhu, F. Zhang, D. Wang, X. F. Pei, W. B. Zhang and J. Jin, *J. Mater. Chem. A*, 2013, **1**, 5758–5765.
9 Z. W. He, D. J. Miller, S. Kasemset, L. Wang, D. R. Paul and B. D. Freeman, *J. Membr. Sci.*, 2016, **514**, 659–670.
10 X. Huang, W. P. Wang, Y. D. Liu, H. Wang, Z. B. Zhang, W. L. Fan and L. Li, *Chem. Eng. J.*, 2015, **273**, 421–429.
11 Y. H. Xiang, J. H. Shen, Y. Z. Wang, F. Liu and L. X. Xue, *RSC Adv.*, 2015, **5**, 23530–23539.
12 S. S. Madaeni, V. Vatanpour, H. A. Monfared, A. Arabi Shamsabadi, K. Majdian and S. Laki, *Ind. Eng. Chem. Res.*, 2011, **50**, 11712–11719.
13 M. M. Tao, L. X. Xue, F. Liu and L. Jiang, *Adv. Mater.*, 2014, **26**, 2943–2948.
14 X. Shen, X. B. Yin, Y. P. Zhao and L. Chen, *Polym. Eng. Sci.*, 2015, **55**, 1367–1373.
15 M. Padaki, R. S. Murali, M. S. Abdullah, N. Misdan, A. Moslehyani, M. A. Kassim, N. Hilal and A. F. Ismail, *Desalination*, 2015, **357**, 197–207.
16 X. Shen, X. B. Yin, Y. P. Zhao and L. Chen, *Colloid Polym. Sci.*, 2015, **293**, 1205–1213.
17 H. Y. Yu, Y. Kang, Y. L. Liu and B. X. Mi, *J. Membr. Sci.*, 2014, **449**, 50–57.
18 Y. Chang, C. Y. Ko, Y. J. Shih, D. Quémener, A. Deratani, T. C. Wei, D. M. Wang and J. Y. Lai, *J. Membr. Sci.*, 2009, **345**, 160–169.
19 H. Takahashi, M. Nakayama, S. Shimizu, M. Yamato and T. Okano, *Biomaterials*, 2011, **32**, 8830–8838.
20 J. Liu, X. Shen, Y. P. Zhao and L. Chen, *Ind. Eng. Chem. Res.*, 2013, **52**, 18392–18400.
21 X. Shen, J. Liu, X. Feng, Y. P. Zhao and L. Chen, *J. Biomed. Mater. Res., Part A*, 2015, **103**, 683–692.
22 R. Xu, Q. Q. Feng, Y. He, F. Y. Yan, L. Chen and Y. P. Zhao, *J. Biomed. Mater. Res., Part A*, 2017, **105**, 178–188.
23 H. Shi, Y. He, Y. Pan, H. H. Di, G. Y. Zeng, L. Zhang and C. L. Zhang, *J. Membr. Sci.*, 2016, **506**, 60–70.
24 X. K. Bian, L. Q. Shi, X. X. Yang and X. F. Lu, *Ind. Eng. Chem. Res.*, 2011, **50**, 12113–12123.
25 A. L. Ahmad, M. A. Majid and B. S. Ooi, *Desalination*, 2011, **268**, 266–269.
26 L. Yan, S. Hong, M. L. Li and Y. S. Li, *Sep. Purif. Technol.*, 2009, **66**, 347–352.
27 S. Zhao, W. T. Yan, M. Q. Shi, Z. Wang, J. X. Wang and S. C. Wang, *J. Membr. Sci.*, 2015, **478**, 105–116.
28 Y. Y. Zhao, J. Q. Lu, X. Y. Liu, Y. D. Wang, J. Y. Lin, N. Peng, J. C. Li and F. B. Zhao, *J. Colloid Interface Sci.*, 2016, **480**, 1–8.

29 A. O. Saf, I. Akin, E. Zorcd and H. Bingol, *RSC Adv.*, 2015, **5**, 42422–42429.
30 X. Yang, Y. He, G. Y. Zeng, Y. Q. Zhan, Y. Pan, H. Shi and Q. Chen, *J. Mater. Sci.*, 2016, **51**, 8965–8976.
31 A. Bottino, G. Capannelli and A. Comite, *Desalination*, 2002, **146**, 35–40.
32 N. Maximous, G. Nakhla, W. Wan and K. Wong, *J. Membr. Sci.*, 2010, **352**, 222–230.
33 Y. M. Zheng, S. W. Zou, K. G. N. Nanayakkara, T. Matsuura and J. P. Chen, *J. Membr. Sci.*, 2011, **374**, 1–11.
34 R. Z. Pang, X. Li, J. S. Li, Z. Y. Lu, X. Y. Sun and L. J. Wang, *Desalination*, 2014, **332**, 60–66.
35 J. Yin and J. C. Zhou, *Desalination*, 2015, **365**, 46–56.
36 S. Haque, I. Rehman and J. A. Darr, *Langmuir*, 2007, **23**, 6671–6676.
37 J. Zhu, X. Z. Zhao and C. J. He, *RSC Adv.*, 2015, **5**, 53653–53659.
38 A. Razmjou, J. Mansouri and V. Chen, *J. Membr. Sci.*, 2011, **378**, 73–84.
39 G. L. Zhang, S. F. Lu, L. Zhang, Q. Meng, C. Shen and J. W. Zhang, *J. Membr. Sci.*, 2013, **436**, 163–173.
40 L. F. Liu, H. P. Chen and F. L. Yang, *Sep. Purif. Technol.*, 2014, **133**, 22–31.
41 E. C. Cho, D. H. Kim and K. Cho, *Langmuir*, 2008, **24**, 9974–9978.
42 J. G. Zhang, Z. W. Xu, W. Mai, C. Y. Min, B. M. Zhou, M. J. Shan, Y. L. Li, C. Y. Yang, Z. Wang and X. M. Qian, *J. Mater. Chem. A*, 2013, **1**, 3101–3111.
43 S. Y. Zhou, A. L. Xue, Y. J. Zhao, M. S. Li, H. Wang and W. H. Xing, *Sep. Purif. Technol.*, 2013, **114**, 53–63.
44 Y. L. Zhang, J. Zhao, H. Q. Chu, X. F. Zhou and Y. Wei, *Desalination*, 2014, **344**, 71–78.
45 M. Safarpour, A. Khataee and V. Vatanpour, *Ind. Eng. Chem. Res.*, 2014, **53**, 13370–13382.
46 L. J. Zhu, L. P. Zhu, Y. F. Zhao, B. K. Zhu and Y. Y. Xu, *J. Mater. Chem. A*, 2014, **2**, 15566–15574.
47 Z. W. Xu, J. G. Zhang, M. J. Shan, Y. L. Li, B. D. Li, J. R. Niu, B. M. Zhou and X. M. Qian, *J. Membr. Sci.*, 2014, **458**, 1–13.
48 Y. Mo, A. Tiraferri, N. Y. Yip, A. Adout, X. Huang and M. Elimelech, *Environ. Sci. Technol.*, 2012, **46**, 13253–13261.
49 X. F. Wang, X. M. Chen, K. Yoon, D. F. Fang, B. S. Hsiao and B. Chu, *Environ. Sci. Technol.*, 2005, **39**, 7684–7691.
50 M. K. Sinha and M. K. Purkait, *Desalination*, 2015, **355**, 155–168.